

A systems biology approach to radiation therapy optimization

Anders Brahme · Bengt K. Lind

Received: 21 December 2009 / Accepted: 24 January 2010 / Published online: 27 February 2010
© Springer-Verlag 2010

Abstract During the last 20 years, the field of cellular and not least molecular radiation biology has been developed substantially and can today describe the response of heterogeneous tumors and organized normal tissues to radiation therapy quite well. An increased understanding of the sub-cellular and molecular response is leading to a more general systems biological approach to radiation therapy and treatment optimization. It is interesting that most of the characteristics of the tissue infrastructure, such as the vascular system and the degree of hypoxia, have to be considered to get an accurate description of tumor and normal tissue responses to ionizing radiation. In the limited space available, only a brief description of some of the most important concepts and processes is possible, starting from the key functional genomics pathways of the cell that are not only responsible for tumor development but also responsible for the response of the cells to radiation therapy. The key mechanisms for cellular damage and damage repair are described. It is further more discussed how these processes can be brought to inactivate the tumor without severely damaging surrounding normal tissues using suitable radiation modalities like intensity-modulated radiation therapy (IMRT) or light ions. The use of such methods may lead to a truly scientific approach to radiation therapy optimization, particularly when *in vivo* predictive assays of radiation responsiveness becomes clinically available at a larger scale. Brief examples of the efficiency of IMRT are also

given showing how sensitive normal tissues can be spared at the same time as highly curative doses are delivered to a tumor that is often radiation resistant and located near organs at risk. This new approach maximizes the probability to eradicate the tumor, while at the same time, adverse reactions in sensitive normal tissues are as far as possible minimized using IMRT with photons and light ions.

Introduction

To accurately describe the radiation response, a tumor and surrounding normal tissues to different therapeutic beams such as sparsely ionizing photons, electrons and protons, or densely ionizing neutrons and light ions, a thorough understanding of the underlying physics and biology is essential. This involves many steps from the functional genomics of the cell and the cell nucleus (Amundson et al. 2003) via the functional arrangement of complex ensembles of cell types in different organs to the often intricate interaction of organ systems (Källman et al. 1992). Some of the key issues in the development of accurate radiation-response models for tumors and normal tissues will be discussed in the present overview.

The growth control and cell cycle regulation as well as the DNA damage surveillance and repair pathways are the key genetic pathways that are involved in human cancer development (Fei and El-Deiry 2003; Nakamura 2004) as well as in the development of the cellular response to ionizing radiations (Nakamura 2004; Brahme 1999, 2004). Today we know that practically all cancers are linked to alterations in key pathways controlling cell growth, cell cycle regulation and DNA damage surveillance and repair (Brahme 1999, 2004). At least one of the gene products of these pathways are affected in all cancers, but generally

Paper presented at First International Workshop on Systems Radiation Biology, GSF Neuherberg/Munich, Germany 2007.

A. Brahme · B. K. Lind (✉)
Department of Medical Radiation Physics, Oncology-Pathology,
Karolinska Institutet, and Stockholm University, P.O. Box 260,
171 76 Stockholm, Sweden
e-mail: Bengt.Lind@KI.se

several genes and pathways are involved. Most often the tumor suppressor and oncogene p53 and its upstream or downstream genes are affected (Fei and El-Deiry 2003) as are the oncogenes Myc and Ras that are involved in the control of cell growth. Interestingly, the same genes are also very important for the cellular radiation response. In tumors where the p53 gene is mutated, the downstream cell signaling is often affected. The common cell cycle block generally induced by p21 through the p53 pathway by Serin15 and Serin20 phosphorylation of the p53 gene product may be lost and, as a result, there is not enough time for repair, and the cell will continue cycling and incorporating damaged DNA in its genome. Furthermore, the apoptotic pathway, often induced by p53 through Serin46 phosphorylation after more severe DNA damage (Nakamura 2004), might also be lost and the tumor can develop hypoxia and resist radiation without an apoptotic response and instead increase its malignancy (Wouters and Brown 1997) or cause secondary cancers (Huang et al. 2003). In fractionated radiation therapy, p53 mutant tumor cells are therefore continuously accumulating more unrepaired damage to their DNA until it occurs in genes important for cell survival, or it results in induction of genetic instability or even mitotic catastrophe. This is probably one of the principal mechanisms in fractionated radiation therapy for eradication of tumor cells in more than 50% of our malignancies that are mutated in p53. At the same time, surrounding normal tissues with wild-type p53 might have well-organized cell cycle blocks and almost complete DNA repair between the daily dose fractions specially if the doses are lower using intensity-modulated radiation therapy (IMRT). In p53 functional tumor cells, the apoptotic pathway may still be functional and lead to effective cell kill particularly by densely ionizing radiation, which generally results in a higher apoptotic fraction (Svensson et al. 2004; Takakura et al. 2004), even in radiation-resistant hypoxic tumors.

It is interesting and, to some extent, it may even be an apparent contradiction that p53 mutant cell lines often seem more radiation resistant in clonogenic cell survival assays than wild-type cell lines, since they loose, for example, less cells through apoptosis (Fei and El-Deiry 2003; Brahme 2004). However, the general response to 30 daily fractions delivered during 6 weeks cannot really be compared to a single irradiation evaluated by clonogenic survival after about 2 weeks. The many fractions leads to a continuous accumulation of damaged DNA in the tumor cell genome, a process that is not generally observable in clonogenic assays with single fractions. The uniquely high curability obtained by using multiple daily radiation fractions against p53 mutant, or more generally, genetically unstable tumors, is thus achieved by repeatedly hitting the Achilles heal of these cells without seriously affecting intact well-organized

healthy normal tissues with well-functioning cell cycle regulation and repair with wild-type p53.

After a brief introduction of some of the new cell survival models that are based on Repairable and potentially Conditionally Repairable damage (RCR) model as described by damage interactions or dual correlated Poisson processes, some sub-cellular eradication processes induced by direct action on the genome are discussed. The RMR (repair–misrepair) cell survival model suggested by Kappos and Pohlit (1972) and Tobias (1985) is interesting, since it describes some possible repair and misrepair events leading to cell survival or inactivation. This idea was continued by Curtis (1986) in the so-called LPL (lethal potentially lethal) model, also based on first principles, showing that in some cases the commonly observed linear quadratic (LQ) cell survival was obtained (Curtis 1986). Today we know that the shoulder of the survival curve is due to repair and that for tissues that may express low-dose hypersensitivity (Marples et al. 2004; Xu et al. 2002), the β term of the LQ model is inaccurate at low and particularly at high doses *cf.* Scholz et al. (1997), Park et al. (2008), Guerrero and Allen Li (2004). Both these problems as well as the accurate description of the ordinary shape of the cell survival shoulder are accurately handled by the recent so-called RCR (repairable-conditionally repairable) model (Lind et al. 2003), and it is briefly described here since it may be closely linked to the two key repair pathways of mammalian cells: Non-homologous end joining (NHEJ) and homologous recombination (HR) (Tachibana 2004; Hoeijmakers 2001). Furthermore, the interaction of different functional subunits in complex organs will be analyzed in detail including hypoxia (Lind and Brahme 2007), sub-cellular targets and the interaction of the responses of different organ systems to radiation therapy. Finally, the application of the radiobiological dose–response models for optimization of radiation therapy will be briefly discussed.

The repairable-conditionally repairable (RCR) cell survival model

The classical linear quadratic (LQ) model ($S(D) = \exp(-\alpha D - \beta D^2)$) suffers from two major problems—at low doses, it does not account for low-dose hypersensitivity, and at high doses, it predicts too much damage due to the βD^2 term. However, the quadratic β term is needed to describe the repair at low doses. The recent RCR model solves these two problems by identifying and considering the two main types of radiation damage: Potentially repairable damage that is mainly repaired by the NHEJ process using DNA-PK and associated genes (Fig. 1, right ellipse in insert). The conditionally repairable damage often requires the fast NHEJ process to work, but also that it is followed by HR working during the late G₂M phase of

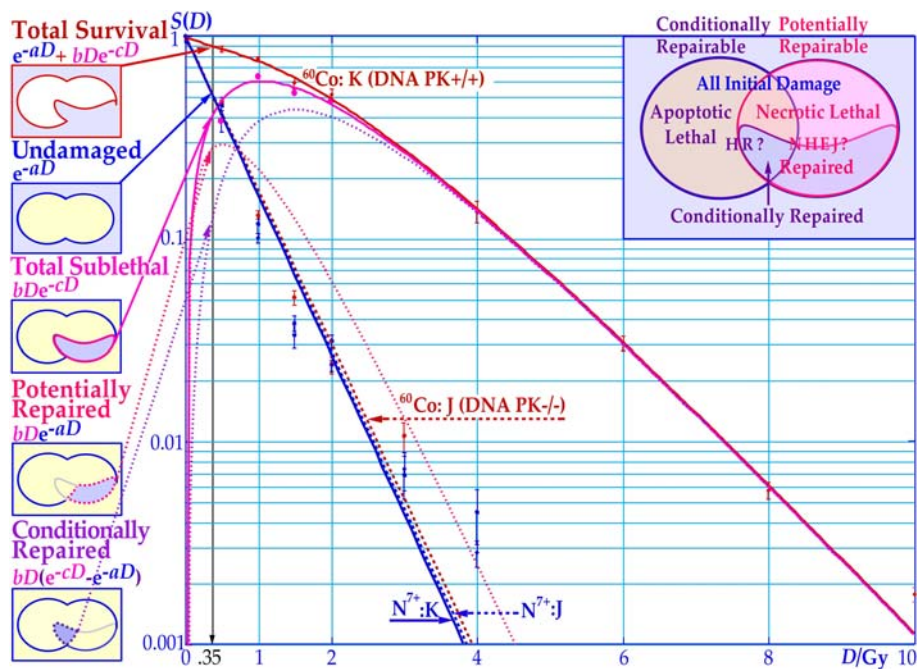


Fig. 1 Description of the cell survival as a function of the absorbed dose in absence of a hit (plain straight exponential survival curves) obtained when most DNA damage cannot be repaired such as in the DNA-PK^{-/-} deficient glioma cells (J) with ⁶⁰Co or when using high-LET N⁷⁺ ions. However, the repairable damage (concave curves) obtained with low LET radiations such as ⁶⁰Co in DNA-PK^{+/+} proficient cells K show a clear shoulder with increasing radiation doses, due to efficient low-LET DNA repair. Interestingly, there was

no difference in cell survival between the two cell lines when they were exposed to nitrogen ions, whereas the response to ⁶⁰Co photon response is very different. This indicates that the high-LET damage of N ions is practically unreparable by DNA-PK in this cell line. In this way, the contributions to the different parts of the cell survival diagrams could be determined experimentally, e.g. at 0.35 Gy, as shown in the left inserts. Interestingly, the conditional repair dominates at high doses. Modified from Lind et al. (2003)

the cell cycle to ensure that possible misrepair caused by NHEJ is as accurately as possible corrected (Fig. 1, left ellipse in insert) (Lind et al. 2003). Interestingly, this two-step process results in a very flexible and yet simple cell survival model if Poisson statistics is applied, describing both low-dose hypersensitivity, the shoulder at about 2 Gy and the mainly exponential tail beyond about 5 Gy as seen in Fig. 1. In this figure, the survival of the human glioma cell lines M059K (DNA-PK_{CS} proficient) and M059J (DNA-PK_{CS} deficient) are shown after exposure to ⁶⁰Co gamma radiation and nitrogen ions. The figure illustrates that potentially repairable damage is repaired by the M059K cells after exposure to low-LET gamma radiation from ⁶⁰Co but not after exposure to high-LET nitrogen ions. The M059J cells can repair neither the sub-lethal damage due to ⁶⁰Co gamma irradiation nor the damage from nitrogen ions allowing quantification of NHEJ-induced repair after ⁶⁰Co gamma irradiation in this cell line. The simple analytical cell survival expression of the RCR model (Lind et al. 2003) is given by:

$$S(D) = e^{-aD} + bDe^{-cD}. \tag{1}$$

The surviving cells in Eq. 1 include those cells that are missed or not damaged (e^{-aD}) and those that are damaged

and then correctly repaired (bDe^{-cD}) after a full recovery time of about 2 weeks (see Fig. 1). The amount of potentially repairable damage is thus—in the first approximation—proportional to the dose (bD), but damage to repaired cells and misrepair may reduce the survival (e^{-cD}). It is also seen in Fig. 2 that the NHEJ process dominates at low doses, whereas at high doses, the conditionally repaired cells dominate the survival since both repair systems are needed. The sub-lethal damage repair could be determined experimentally for those cell lines capable of NHEJ repair (M059K) by subtracting the cell survival of DNA-PK knockout cells (M059J) that only results in survival with essentially undamaged cells that survives independent of any repair system. Thus, the HR process becomes important at higher doses and later time points when the probability for multiply damaging local events increases. Interestingly, this model can handle the interaction of events characterized by low and high LET in a very accurate manner as data on X-ray and neon exposure demonstrate (Lind et al. 2003).

Based on the cell survival curve of the RCR model (or any other survival model like the L or LQ model), it is straightforward to derive the response of a homogeneous or heterogeneous tumor to fractionated radiation therapy as

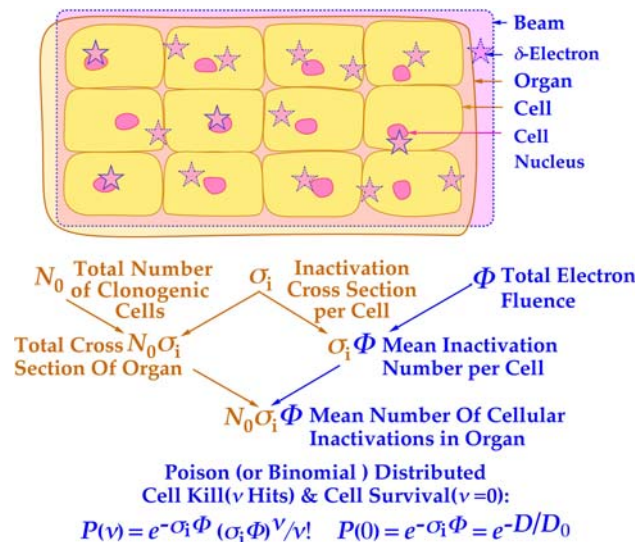


Fig. 2 The damage to a tissue or a tumor is composed of the probability to damage each of its constituent cells, or in a more complex organ by damage to its functional subunits. For practically all radiation modalities, the fluence of low-energy delta rays is causing most of the lethal damage. Poisson, or more generally Binomial statistics, when the number of functional subunits is small, can often be assumed as shown in the figure and in Fig. 3

shown in Figs. 2 and 3 (Källman et al. 1992; Brahme 1999). Figure 3 clearly demonstrates how a cell survival curve (the ridge of the Binomial distribution), even with low-dose hypersensitivity, is transformed to a sigmoidal Poisson type dose–response curve at high doses and low survival levels, and with a high probability to eradicate all tumor cells at high doses ($\lim_{n \rightarrow \infty} P_B = 1$). The cell survival curve and the dose–response relation (cf. Fig. 3) of even a very heterogeneous tumor with a wide spectrum from quite sensitive to very resistant cells can be accurately approximated by two effective components, one describing the sensitive compartment (N_s) and one the resistant compartment (N_r) as demonstrated more clearly in Fig. 4 cf. (Lind and Brahme 2007). The resistant fraction is often determined by hypoxic or otherwise radiation-resistant cells, whereas the sensitive compartment is generally well oxygenated. The mean number of surviving cells $\bar{N}(d, n)$ after n dose fractions would then be of the type:

$$\bar{N}(d, n) = (N_s(e^{-a_s d} + b_s d e^{-c_s d})^n + N_r(e^{-a_r d} + b_r d e^{-c_r d})^n). \tag{2}$$

where a_s, b_s and c_s are the sensitive and a_r, b_r and c_r are the resistant cell survival parameters and N_s and N_r are the initial number of sensitive and resistant cells, respectively. According to the Poisson model, the probability to eradicate such a tumor would then be

$$P_B(d, n) = e^{-\bar{N}(d, n)}. \tag{3}$$

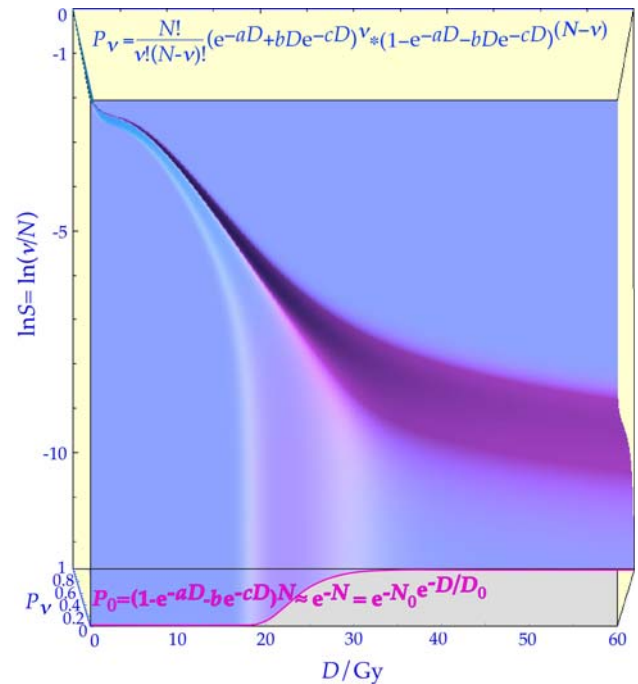


Fig. 3 Description of the Binomial cell survival in a three-dimensional diagram where the vertical axis expresses the probability for a given cell survival after irradiation (upper Binomial equation). The RCR cell survival with low-dose hyper sensitivity is clearly transformed here to a dose–response curve at very high doses where the more complex Binomial model is well approximated by the exponential dose–response relation of the Poisson model (lower Poisson equation, see also Fig. 2)

This function is shown in Fig. 3 for a uniform tumor, and for fractionated irradiation of a heterogeneous tumor in Fig. 4. In the following sections, we will discuss some subcellular processes that will influence cell survival.

Loss of clonogenicity due to essential gene inactivation

When a clonogenic cell is exposed to ionizing radiation it may lose its clonogenic ability by a large number of damaging processes, some of which might be truly lethal while others might be repairable, conditionally repairable or senescent (Lind et al. 2003). The dominating damage type produced by low ionization density or low-LET radiations is caused by direct or indirect, radical mediated, damage to nuclear DNA. Most of this latter damage is repairable and—on average—it corresponds to about 35 double strand breaks per cell at 1 Gy, and approximately 20 times as many easily repairable single strand breaks. Only a few percent of the induced double strand breaks are lethal and inactivate the cell with a probability of approximately 50% at 2 Gy (survival fraction at 2 Gy— $SF_2 \approx 0.5$). It is interesting to note that for low-LET

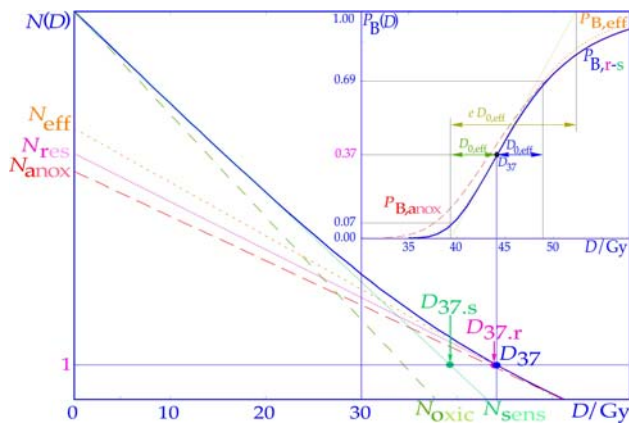


Fig. 4 The variation of the amount of cell kill with increasing dose for a strongly Heterogeneous tumor. At low doses, the radiation-sensitive (N_s) and well-oxygenated (N_o) tumor cells dominate the cell kill, whereas at high doses the remaining radiation-resistant (N_r) or anoxic (N_a) tumor cells dominate the response. The sensitive component responds similar as the oxic component (N_{oxic}) whereas the resistant component is similar to the anoxic component (N_{anox}). N_{eff} is the effective number of cells approximately describing the dose–response curve ($P_{B, eff}$, dotted curve) at intermediate doses. The dose D_{37} is causing 37% ($1/e$) tumor control and is given where in average one cell of any type is surviving due to Poisson statistics (cf. Eq. 3). $D_{0,eff}$ is the effective dose reducing the cell survival to 37% or $1/e$

radiation this is approximately equal to the probability of having one low-energy δ -electron in the energy range between 100 and 1,000 eV being imparted in the cell nucleus. Such low-energy δ -electrons are characterized by a very dense energy deposition that may result in about five single and double strand breaks within a region of about 10 nm in diameter. The corresponding local dose is in the order of MGy, and the track average LET is of the order of 50–70 eV/nm over a few nm. It is very likely that these electron track ends are responsible for a large part of the lethal damage in the form of multiple damaged sites (Ward 1984; Michalik and Frankenberg 1994) that most commonly occur in the form of dual nucleosomal double strand breaks (Brahme et al. 1997). The repair process induced at these track-end sites stimulate DNA de-condensation in larger regions to facilitate repair and may also cause chromosome–chromosome cross-links that are lethal during cell division.

At higher LETs, the proportion of δ -electrons is even higher. These electrons are generated at an increasing density toward the Bragg peak and are thus increasing the biological effectiveness of high-LET radiations. This will also increase the risk for other lethal effects such as membrane damage or damage to other essential sub-cellular organelles such as the mitotic spindle. At high LET, an increasing proportion of the slowing down spectrum consists of δ -electrons and ion fragments which predominately produce secondary electrons in the keV and sub-keV

range. Ions produce particularly high local energy deposition densities, since subsequent secondary electrons are strongly correlated in space both through their radial convergence on the ion path and since they are generated at denser intervals towards the Bragg peak. The high dose at the Bragg peak region is characterized by a velocity resonance making the energy transfer from the ion to orbital electrons very high when the ion velocity approaches that of the orbital electrons.

Some of the lethal damage may cause definite cell death through an apoptotic response. This response might be due to DNA damage through the p53-dependent pathways or by p53-independent action such as membrane damage through the ceramide pathway (Brahme 2004). The former processes can probably be triggered in all kinds of DNA, whether the DNA contains functionally transcribing genes or not. Loss of clonogenicity may also be caused by senescence (permanent cell cycle arrest) and inter-chromosomal cross-links which are very difficult to repair by the cell. One should also quantify the probability of inducing a lethal response by damage induction anywhere in the genome, for example through apoptosis. A less investigated loss of clonogenicity may be induced by fatal damage to all alleles of a gene essential for clonogenic survival. In the G_0 and G_1 cell cycle phases, there should be two independent alleles, one from the father and one from the mother. Other genes may be heterozygous so one allele is missing or damaged, and still others may exist in multiple copies due to gene amplification. Furthermore, during the S phase all genes are being duplicated and, as a result, during the late G_2 and early M phases there should be exactly two alleles from each parent. To calculate the probability of a lethal event of this type where an essential gene is lost, one needs to calculate the probability to inactivate a pair of alleles of any gene that is essential for clonogenic survival.

Let us first look at the genome of a normal diploid cell, which consists of 3×10^9 base pairs (bp) of which only a few percent are located in functionally encoding genes. The functionally encoding genome is therefore about 10^8 bp over which about 22,300 genes are distributed. Thus, the average gene size is in the order of 5 kbp. Assuming that each nucleosome contains about 180 bp, this corresponds to about 25 nucleosomes per gene or to a chromatin length of 40 nm. Given the fact that the chromatin fiber has a diameter of 30 nm, in its compacted form the average gene may therefore be enclosed by a sphere of a about 40 nm diameter.

In Fig. 5, two different essential genes (cyclin D and MDM2) are visualized by fluorescence in situ hybridization (Multicolour FISH). It is clearly seen that the two alleles of each gene are generally located about half a nuclear diameter apart, since they are normally placed on separate chromosomes. Modeling gene inactivation by an ion beam

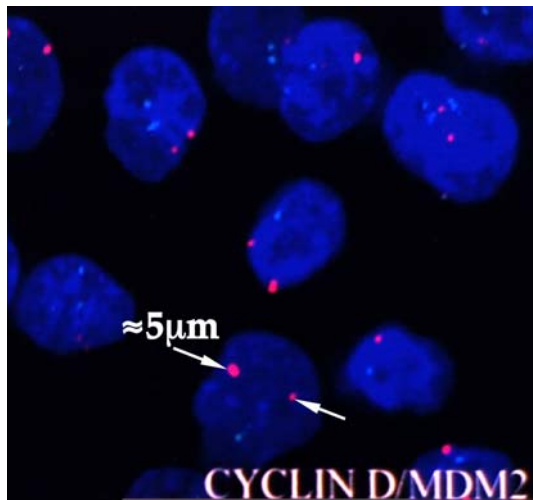


Fig. 5 Two different genes were painted by the FISH technique showing that some tumor cells may miss one allele or have gene amplification and that the normal paternal and maternal alleles are often located at fairly large distance from each other

can therefore be reduced to the problem of having an ion traversal through the cell nucleus where almost at the same time a secondary electron may inactivate the first allele, and a fraction of a pico second later another secondary electron inactivates the complementary allele as indicated in Fig. 6. Obviously, the lower probability that a second ion inactivates the complementary allele also has to be considered.

The damage clusters from the large number of ion generated sub-keV δ -electrons are very dens. This is illustrated in Fig. 7. If these electrons hit the periphery of a nucleosome, two double strand breaks and four free DNA ends are commonly produced. With four free DNA ends at the periphery of a nucleosome, there is not enough space for the KU70 and KU86 gene products needed for repair

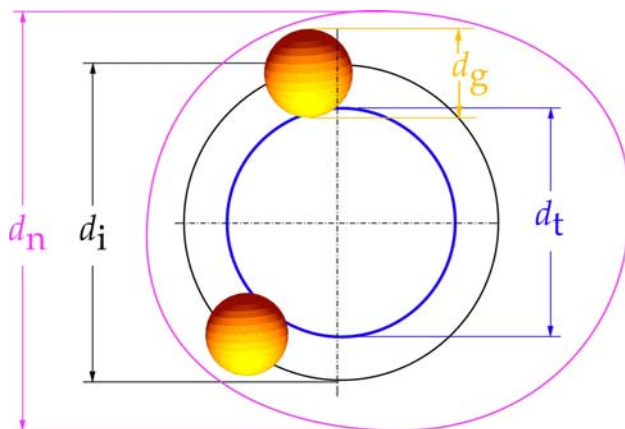


Fig. 6 Looking down along an ion track, it is shown how an ion path can have a high probability to eradicate both the maternal and paternal alleles of key genes. The effective diameters of the different components inside the cell nucleus can be used to estimate the eradication probability as discussed in Eqs. 4–9

using NHEJ, to bind to all the free DNA ends. This makes repair difficult, at least by the NHEJ process. Therefore, the eight histones of the nucleosomes have to be disassembled to provide full access for the KU gene products. Expression of γ H2AX is known as one of the earliest events after exposure to ionizing radiation. When the nucleosomes are dismantled, it is not unlikely that the exact relation between the quasi-free DNA ends may be lost resulting in, for example, free DNA strands or loops of around 78–80 bp that correspond to the length of one turn around the nucleosome (Brahme et al. 1997). If the risk for misrepair is not handled well, e.g. by the high-fidelity sister chromatid exchange process during the S phase or by the HR process during the G_2 –M transition, permanent lethal damage may result. This conditional repair mechanism may be the reason for low-dose hypersensitivity and the shouldered shape of the cell survival curves for low-LET radiations (Lind et al. 2003).

To quantify the risk for such events, the geometrical relations in Fig. 6 may be used. The risk for severe damage to both alleles of an essential gene is determined by the probability of any pair of alleles of any of the essential genes to be hit by the passage of one or possibly—but much more unlikely—by two independent ions (see Eq. 9). The inactivation probability for randomly located alleles is on the average given by the probability of a lethal overlap configuration between both alleles of any of the essential genes and the lethally damaging core of randomly traversing ions. If we call the mean diameter of the gene d_g , the mean diameter of the cell nucleus d_n , and the mean diameter of the lethal damage zone of the ion track d_t as shown in Fig. 6, the mean cord length of the ion in crossing the cell is then

$$\bar{l} = 4V_n/A_n = 4 \cdot \frac{4}{3} \pi r_n^3 / 4\pi r_n^2 = \frac{2}{3} d_n, \quad (4)$$

where r_n denotes the radius, V_n the volume and A_n the surface area of the cell nucleus n . The nuclear volume, V_n , the track volume V_t and the gene volume V_g are then given by

$$V_n = \frac{4\pi r_n^3}{3} = \frac{\pi}{6} d_n^3, \quad (5)$$

$$V_t = \pi r_t^2 \bar{l} = \frac{\pi d_t^2}{4} \frac{2}{3} d_n = \frac{\pi}{6} d_t^2 d_n, \quad (6)$$

and

$$V_g = \frac{\pi}{6} d_g^3. \quad (7)$$

For simplicity, it may be assumed that a lethal inactivating event requires that both alleles are hit by the same ion core, that is, the center of both alleles has to be inside a cylinder of a diameter, d_i given by the sum of the diameters of the

Fig. 7 Sub-keV electron track ends are the most lethal events capable of inducing dual nucleosomal double strand breaks that are very difficult for the cells to repair. The Ku70 and Ku86 molecules that first bind to the free DNA ends during repair can only do so after the histone octamers of the nucleosome has been dismantled. Then, the probability to lose a whole DNA turn around the nucleosome (~78 base pairs) is very high as seen from the lower right insert showing the distribution of DNA fragments after irradiation to a mean dose of 40 Gy (cf. (Brahme et al. 1997)). Track-end-induced dual nucleosomal double strand breaks may therefore be one of the most probable lethal events both at low and high LET

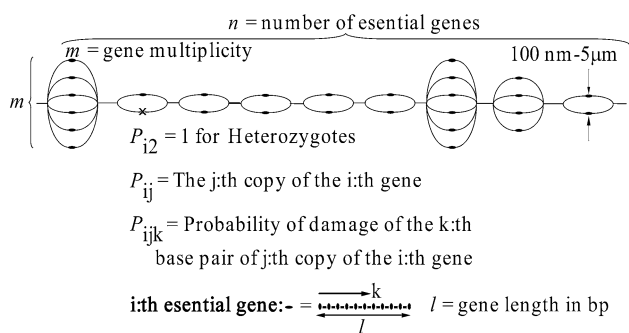
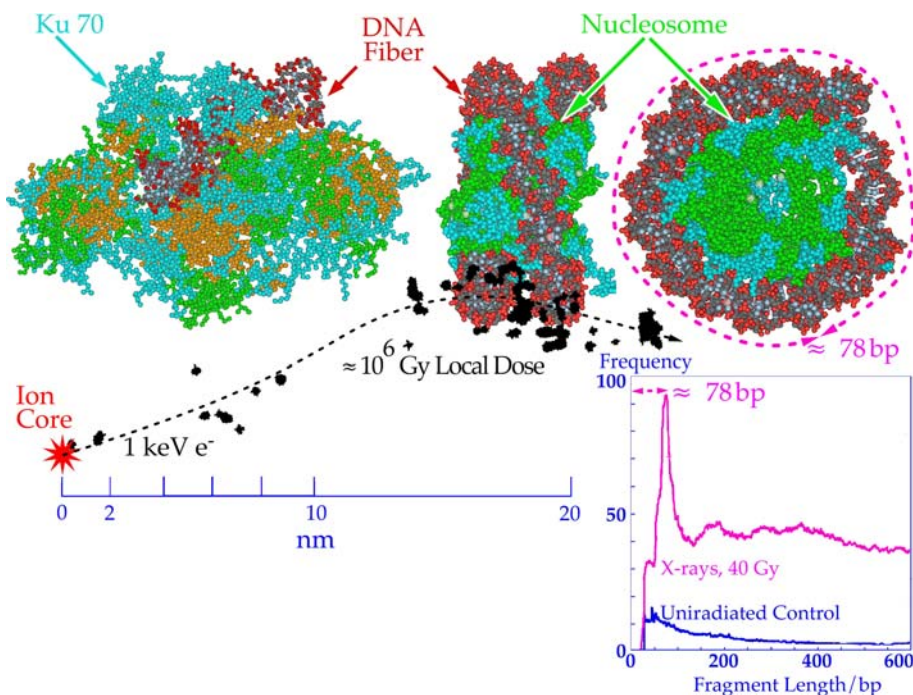


Fig. 8 Description of the functional organization of key genes essential for cell survival. Since these are essential for survival, they are functionally organized in series, even if they may be located at different chromosomes. Some of these genes may be heterozygotes or imprinted with a single active copy, but most are normal and are available in two copies, functionally organized in parallel, whereas others may be amplified up to m -fold multiplicity. In this way, single SNPs and CNPs can be taken into account when estimating the probability for cell kill

gene and the lethal core $d_i = d_t + d_g$ (Fig. 6). If all alleles are located inside the cell with uniform probability, the mean probability of allele inactivation per ion passage is given by the ratio of the inactivating volume V_i and the total nuclear volume V_n according to:

$$P_0 = \frac{V_i}{V_n} = \frac{\frac{\pi}{6}d_n(d_t + d_g)^2}{\frac{\pi}{6}d_n^3} = \left(\frac{d_t + d_g}{d_n}\right)^2 \quad (8)$$

If both alleles are hit by independent ion cores, the corresponding probability can be calculated by the product of the probabilities of each event given by Eq. (8) (if the

events are assumed to be statistically independent and both are needed for lethality):

$$P_g = \left(\frac{d_t + d_g}{d_n}\right)^4 \quad (9)$$

In addition, each event has to be multiplied by the probability of having one or more ion traversals, respectively.

The above-mentioned formulae clearly represent an approximative estimate of the true probability for lethal damage. A more accurate estimate would require to average more accurately over all possible ion paths and their associated secondary electron “trees” relative to the associated essential allele locations. This could only be done with rather complex Monte Carlo or Vegas type calculations. In addition, the cells can also be inactivated by chromosomal cross-links and by an induced apoptotic response anywhere in the DNA, not just in the functionally important genes.

From the above-mentioned expression, it is possible to derive the total inactivation probability considering all essential genes N_g , their individual allele multiplicity m_g , and the distribution of the number of ion traversals in each nucleus. The mean number, \bar{n} , of ions traversing a cell nucleus is largely governed by Poisson statistics

$$\bar{n} = \Phi \frac{\pi d_n^2}{4}, \quad (10)$$

where Φ is the ion fluence which is related to the dose through $\bar{D} = \Phi \frac{\bar{L}_\Delta}{\rho}$, where \bar{L}_Δ is the fluence mean restricted LET, and ρ is the density. The probability for precisely n ion passages is thus given by (cf. Fig. 3)

$$P_n = \frac{e^{-\bar{n}} \bar{n}^n}{n!} \tag{11}$$

If we assume there are N_1 heterozygotic or imprinted genes with only one active allele, N_2 normal diploid genes and N_m genes of multiplicity m as shown in Fig. 9, the total number of functional alleles is given by

$$N_a = \sum_{i=1}^M iN_i, \tag{12}$$

and the total number of genes is given by

$$N_g = \sum_{i=1}^M N_i, \tag{13}$$

where M is the maximum gene multiplicity.

Thus, the relative probability to hit an allele of multiplicity m is given by

$$P_m = \frac{m}{N_a} = m / \sum_{i=1}^M iN_i. \tag{14}$$

The probability to have precisely v_1 hits of gene one, v_2 hits of gene two etc., is now given by the polynomial theorem if one sets $N = v_1 + v_2 + \dots + v_{N_g}$, that is the total number of hits according to:

$$P_{v_1, v_2, \dots, v_{N_g}} = \frac{N!}{v_1! v_2! \dots v_{N_g}!} P_{1, m_1}^{v_1} P_{2, m_2}^{v_2} \dots P_{N_g, m_{N_g}}^{v_{N_g}}, \tag{15}$$

where $P_{1, m_1} = \frac{m_1}{N_a}$ and so on. We can now set up the expression for cell inactivation with all the N_g genes of different multiplicity and ion traversal probability:

$$\begin{aligned} P_i &= P_1 (N_1 P_a + N_2 P_a^2 + \dots + N_m P_a^m) \\ &+ P_2 (N_1 (2P_a - P_a^2) + 2N_2 P_a^2 (2P_a - P_a^2)^2 + \dots) \\ &+ P_3 (N_1 (3P_a - 3P_a^2 - P_a^3) \\ &+ N_2 (3P_a - 3P_a^2 - P_a^3) + \dots) + \dots \\ &= \bar{n} e^{-\bar{n}} P_a \left[N_1 \left(1 + \bar{n} \left(1 - \frac{P_a}{2} + \frac{\bar{n}}{2} + \dots \right) \right) \right. \\ &\left. + N_2 P_a \left(1 + \bar{n} \left(1 + \left(1 - \frac{P_a}{2} \right) \right) + \frac{\bar{n}}{2} \right) + N_3 P_a^2 \dots \right] \end{aligned} \tag{16}$$

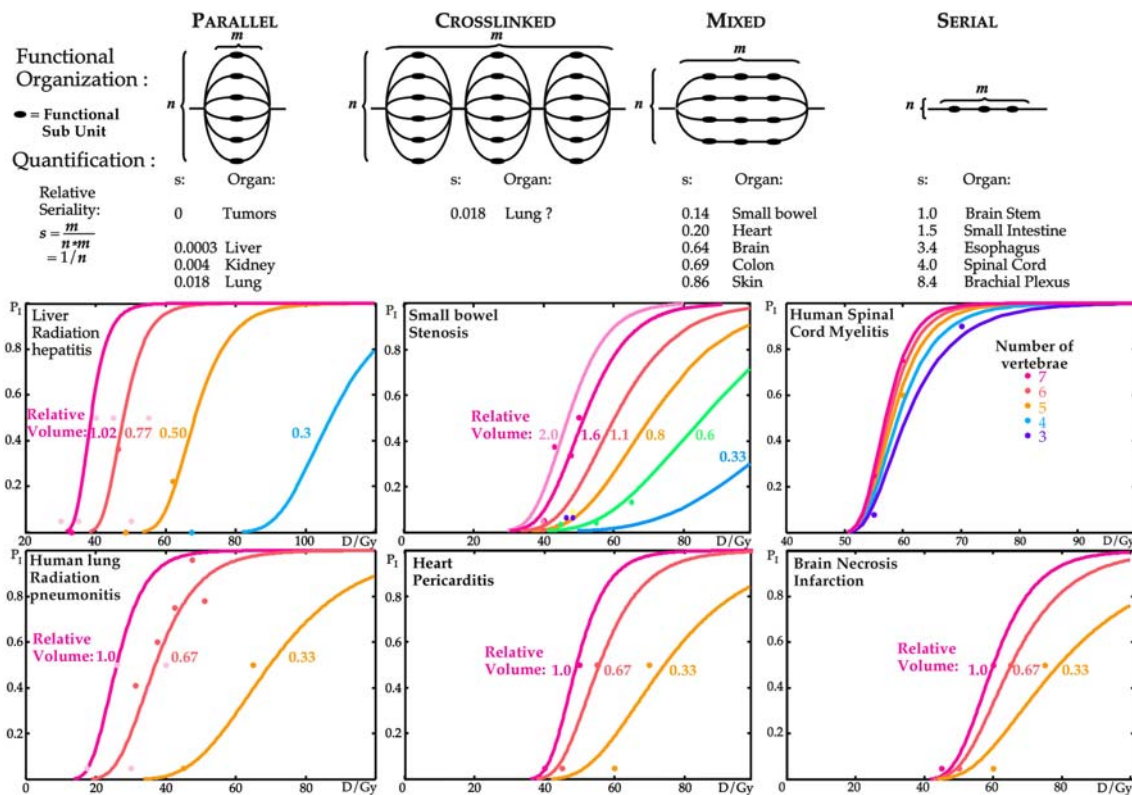


Fig. 9 Influence of the functional organization of different tissues on their dose–response relation. The volume dependence of the shape of the dose–response curves for different normal tissue types is strongly depending on their functional organization (cf. Fig. 8 for that of the cell nucleus). The response of serial tissues like the spinal cord is almost independent on the irradiated volume, whereas parallel organs like the kidney and the lung can tolerate very high doses to small parts

of their volumes (see text). Serial tissues and single cells (cf. Fig. 8) are therefore most sensitive to the highest dose value to the tissue or cell, whereas parallel tissues (low relative seriality) are more sensitive to the mean dose deposited in the organ. The dots are clinical data fitted to an analytical dose–response relation (cf. 3 and Brahmé (1999))

It is thus seen that the normal diploid and the essential but heterozygote genes dominate the cell inactivation probability. At normal therapeutic doses, \bar{n} is low enough for multiple events to show a reduced probability. It is also seen that straight ion paths through a cell nucleus show a higher probability for inactivation than the randomly distributed lethal ionizations obtained at low ionization densities.

Influence of microscopic dose variations on the gene level

In the case of classical low-LET radiations such as photons, electrons and protons the microscopic energy deposition is rather homogeneous on a scale comparable to the size of the cell nucleus. The coefficient of variation of the absorbed dose to the cell nucleus ($\sim 8 \mu\text{m}$ diameter) is generally below 1% at curative doses around 65 Gy. For high-LET radiation, however, the value of the relative biological effectiveness (RBE) is often around 3, the curative absorbed dose around 22 Gy, and the microscopic coefficient of variation on the cellular level as high as 10–15% for neutrons and neon ions. Therefore, by increasing the high-LET component, the micro-dosimetric variance in the cell nuclei is generally increased. This effect has been quantified for its clinical effects on the dose–response relation (Lindborg and Brahme 1990; Tilikidis and Brahme 1994) based on the mean dose and the microscopic standard deviation of the dose on the scale at the cell nucleus. In order to quantify the radiation response on the subcellular level more accurately, a number of simplifying assumptions must be made:

1. The critical subcellular targets are the DNA of key gene pairs for important cellular functions. These are assumed to be quasi-uniformly distributed throughout the cell nucleus.
2. The two alleles of each gene are typically separated by a characteristic distance d of a few μm . This roughly corresponds to the radius of the cell nucleus, but it can vary from gene to gene and also during the cell cycle.
3. A critical target is inactivated if both alleles of a gene that is important for cellular function are functionally damaged.
4. As a first approximation and for simplicity, all alleles are assumed to be equally large, and therefore, essentially of the same sensitivity.
5. The cell loses its proliferative capacity if one or more of these critical genes, or more generally, paired nuclear targets are inactivated.
6. Imprinting, non-functional alleles in heterozygote patients will generally increase the probability for loss

of heterozygosity, whereas gene amplification may result in a significantly decreased tumor response. These effects are disregarded here for simplicity.

7. The difference between recessive and dominant genes are generally of minor importance, possibly except for tumors where dominant proto-oncogenes and recessive tumor suppressor genes may significantly affect the response. These factors are also disregarded here.

There are some 22,300 actively coding genes in the human genome consisting of a total of 3×10^9 base pairs of which only a few percent are located in actively coding genes. The average gene size is therefore around 5×10^3 base pairs, but there is a fairly large variability in gene size. The exact number of intact genes required for clonogenic survival is not known, but probably a considerable fraction of the above figure. Fortunately, the exact number is not important for the present analysis since a normalization to clinically observed responses can be made. Therefore, it should be possible to determine this number indirectly from cell survival data. Since all essential genes have to be intact to support the clonogenic capability of a cell, they are functionally organized in series as shown in Fig. 8. However, for each gene, the allele from the father and mother respectively have similar function. They are therefore functionally arranged in parallel. For this reason, it is possible to create a functional organization map of the genome similar to the maps previously made for normal and tumor tissues (Källman et al. 1992) to calculate the microscopic and sub-cellular radiation response.

If the absorbed doses to the two alleles of the essential gene i are denoted by D_{i1} and D_{i2} , and their inactivation probabilities by $P_i(D_{i1})$ and $P_i(D_{i2})$, respectively, then the total probability to inactivate at least one out of n such pairs is given by

$$P(\mathbf{D}) = 1 - \prod_{i=1}^n (1 - P_i(D_{i1})P_i(D_{i2})), \quad (17)$$

where \mathbf{D} is the total microscopic dose distribution vector $\mathbf{D} = (D_1, D_2, \dots, D_n)$ describing the mean dose distribution to all genes inside the cell nucleus. If the cell nucleus is irradiated with a homogeneous dose D instead, also on the microscopic level, the total inactivation probability becomes simply:

$$P(D) = 1 - \left(1 - P_i(D)^2\right)^n, \quad (18)$$

if we, for simplicity, assume that all essential genes to have the same size and sensitivity. Unfortunately, there is no radiation modality that would allow exposure of the genes to a perfectly uniform absorbed dose, due to the stochastic nature of the energy depositions by ionizing radiation. The lowest possible micro-dosimetric standard deviation is

obtained by high-energy electrons with a coefficient of variation of 0.7% over the 8 μm diameter of the cell nucleus at curative doses of about 65 Gy (Tilikidis and Brahma 1994; Lindborg and Brahma 1990). High doses of high-energy electrons are therefore the best way to generate a dose distribution that is as uniform as possible, inside a cell nucleus. For a more accurate analysis, the exact statistical distribution at the mean absorbed dose to the different alleles should ideally be accounted for. Eq. 18 can be solved for $P_i(D)$

$$P_i(D) = \left(1 - (1 - P(D))^{1/m}\right)^{1/2}. \quad (19)$$

Substituting Eq. (19) back in Eq. (17) to account for the varying dose distributions of ions (*cf.* (Källman et al. 1992)) gives

$$P(D) = 1 - \prod_{i=1}^n \left\{ 1 - \left[\left(1 - (1 - P(D_{i1}))^{1/n}\right) \times \left(1 - (1 - P(D_{i2}))^{1/n}\right) \right]^{1/2} \right\}, \quad (20)$$

where $P(D_{i1})$ and $P(D_{i2})$ are the probabilities to inactivate the cell when receiving the doses D_{i1} and D_{i2} , respectively. Since the probability of survival is given by $S(D) = 1 - P(D)$, the total probability of cellular survival after exposure to an arbitrary non-uniform dose distribution is given by

$$S(D) = \prod_{i=1}^n \left(1 - \left(\left(1 - S(D_{i1})^{1/n}\right) \left(1 - S(D_{i2})^{1/n}\right) \right)^{1/2} \right), \quad (21)$$

where $S(D_{i1})$ and $S(D_{i2})$ are the survival probabilities when the whole cell nucleus receives the homogeneous doses D_{i1} and D_{i2} , respectively. By using $S = \exp(\ln S)$, Eq. (21) can be rewritten as a sum according to

$$S(D) = \exp \left(\sum_{i=1}^n \ln \left(1 - \left(\left(1 - S(D_{i1})^{1/n}\right) \times \left(1 - S(D_{i2})^{1/n}\right) \right)^{1/2} \right) \right). \quad (22)$$

Due to the stochastic nature of the energy deposition on the microscopic level, the doses to the two alleles of gene i , D_{i1} and D_{i2} , can be regarded as a sample i from two stochastic variables, each with the same expectation value $\bar{D} = ED_1 = ED_2$ and variance $\sigma_D^2 = VD_1 = VD_2$. However, the correlation coefficient $\rho(d) = C(D_1, D_2)/\sigma_\mu^2$ will be non-zero and depend on the characteristic distance between and orientation of the two alleles relative to particle tracks as well as the autocorrelation function between energy depositions at a distance d along the tracks. The exponent in Eq. (22) can thus be interpreted as an expectation value of the stochastic variables D_1 and D_2 .

Influence of microscopic dose fluctuations on the base-pair level

It is well known that a single base-pair mutation is sufficient to transform a normal cell into a tumor cell or to a cell without clonogenic capability. To be more strict, it may therefore be desirable to bring the microscopic considerations down to the base-pair level. The size of each gene and its possible amplification status has thus to be taken into account. However, in the following discussion, for the sake of simplicity, instead each base pair is assumed to have the same sensitivity or risk of getting damaged. Let P_{ijk} denote the inactivation probability of the k th base pair at the j th allele of gene i , then in analogy with Eq. (17) the cellular inactivation probability can be written as:

$$P = 1 - \prod_{j=1}^n \left[1 - \prod_{i=1}^m \left(1 - \prod_{k=1}^l (1 - P_{ijk}) \right) \right], \quad (23)$$

where l is the total length in base pairs of the j :th allele of gene i , m is the total multiplicity of gene i , and n is the total number of genes essential for clonogenicity (*cf.* Fig. 8). It is seen from Eq. (23) that all base pairs are assumed to be functionally arranged in series, whereas the amplified genes are all in parallel. In general $m = 2$, while it is 1 for zygotic cells and for heterozygotes. Furthermore, for some base pairs $P_{ijk} \equiv 1$, since they will not be critical with regard to the function of the protein they are coding for. Similarly, for all single nucleotide polymorphisms (SNPs) the same sensitivity is assumed which may not be true in reality. Finally, m may be larger than 2 for gene amplification, copy number polymorphisms (CNPs) and multiploidal cells. If it is again assumed for the sake of simplicity that all genes exist in two intact alleles of length l_n for gene n and that the survival of each base pair, S , is small, then at dose D

$$P_{ijk} = 1 - S(D) \quad (24)$$

and thus the cellular survival $S(D)$ is given by

$$S(D) = \prod_{j=1}^n [1 - (1 - S^{l_n}(D_{j1}))(1 - S^{l_n}(D_{j2}))]. \quad (25)$$

For a uniform dose, an allele multiplicity of 2, and constant fixed gene length l , it is possible to solve for the base-pair survival

$$S^l(D) = \left(1 - \left(1 - S(D)^{1/n} \right)^{1/2} \right)^{1/2}.$$

From the mathematical form of this expression and from standard cellular survival curves $S(D)$, it is clear that extremely high doses of the order of 1 or 10 MGy and more have to be given, in order to damage a given nucleosome or base pair, respectively (Brahme et al. 1997). From the last

few sections, it is evident that there are many different inactivation processes that can lead to cell kill, and the response will be quite different for low- and high-LET radiations.

Tumor and normal tissue responses

Independent of the sub-cellular inactivation, the sigmoidal cell survival at high doses is very characteristic for tumor eradication as seen in Figs. 3 and 4, and a similar curve can generally be observed for most side effects of normal tissue as seen in Fig. 9. However, in this case, the curve shape is a more complex function of the functional organization of the tissue, since some organs are of essentially parallel organization, such as the kidney where all nephrons together help in purifying the blood. On the contrary, in the spinal cord, all the myelin sheets and oligodendrocytes have to be intact as well as the Kinesin engines that refurbish axon function (Adamus-Górka et al. 2008; Hirokawa and Takemura 2005). To assure correct signal transduction, this tissue requires that all its components are intact and thus they are functionally organized in series. This results in a quite different variation of the response with the volume irradiated for these two tissues as seen in Fig. 9. Most normal tissues have a functional organization somewhere between the two extremes of a purely serial and parallel tissue (cf. Fig. 9). This mixture can be described by their relative seriality that reaches values close to zero for strongly parallelly organized organs (Källman et al. 1992). For the lung, where different groups of alveoli work together and partly form a parallel or cross-linked structure as shown in Fig. 9. Such a cross-linked structure may therefore be a more realistic description than a purely parallel structure for some regions of the lung.

As seen in Fig. 9, serial tissues show a very stable dose–response relation, since adding more myelin sheets to the length of cord being irradiated does not really change the risk for paralysis very much. The segment with highest dose is most critical. On the contrary, kidney, liver and lung, that are of strongly parallel organization, tolerate a very high dose in a small volume, since the rapid recovery of parallel subunits exposed to low doses compensate for the local loss of subunits exposed to high doses. It is thus easier to treat a tumor located near or inside a parallel organ than a tumor located close to a serial organ at risk. An accurate description of the responsiveness of different normal tissues is thus essential for treatment optimization for example in terms of minimal damage in normal tissues and maximum probability of cell killing in tumor tissue.

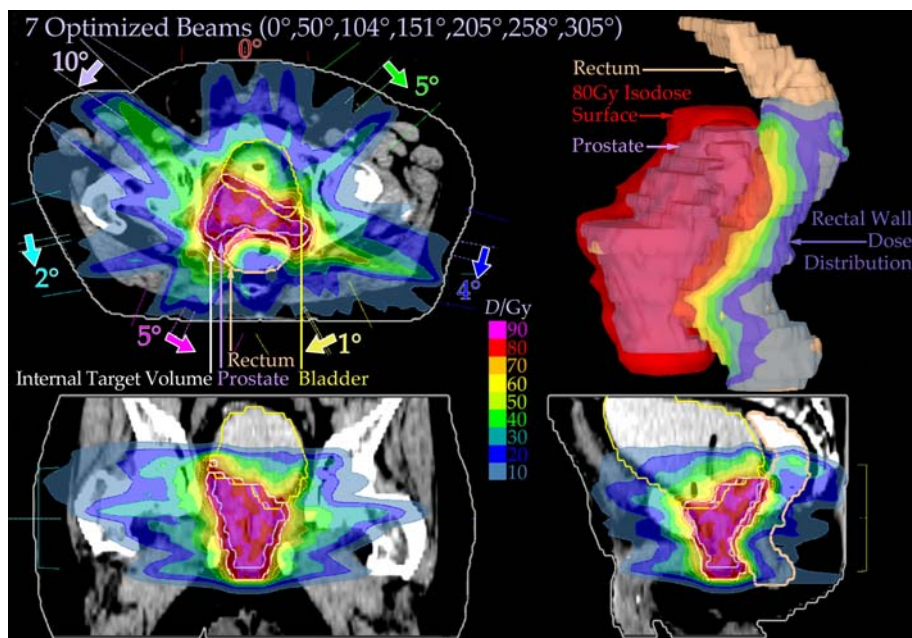
Based on Eq. (2), it is possible to describe the response of complex tumors and normal tissues with significant hypoxia. Since hypoxia represents, in the first approximation, a dose-modifying effect, the resistant and sensitive response parameters can approximately be related to the effective oxygen enhancement ratio (*OER*) such that for the RCR model $a_r \approx OER \cdot a_s$ (cf. Eq. 2). Since the well-oxygenized cell compartments are most radiation sensitive, they will dominate the response at low doses, whereas the more radiation-resistant hypoxic compartments will be dominating at high doses as seen in Fig. 4 (cf. (Lind and Brahme 2007)). Figure 4 also shows how the cellular response to complex hypoxia distributions located at different distances from the vascular tree can very accurately be approximated by a two component model like Eq. (2). For simplicity, it is assumed in Fig. 4 that fractionated treatments are used. In this case, the more complex RCR expression can be approximated by a more simple exponential expression assuming that the dose per fraction, d , is constant so $S(D) = N_r \exp(-D/D_r) + N_s \exp(-D/D_s)$, where $D_r = -d / \ln(\exp(-a_r d) + b_r d \exp(-c_r d))$ and D_s is given by a similar expression in which r is replaced by s . These effective radioresistance parameters, D_r and D_s , are differing by a fraction of a Gy from the values for the pure anoxic and oxic cell compartments as seen by the N_r and N_s compartments in Fig. 4 and (Lind and Brahme 2007).

When in average one clonogenic tumor cell survives, the probability of cure, *i.e.* no surviving tumor cells, is also $\exp(-1)$ or 37% (due to Binomial statistics as seen in the insert of Figs. 2 and 4). It is also seen that the initial slope is shallower than that of the well-oxygenated cells, whereas at high doses, a slightly steeper response than for the anoxic cells is observed. A single effective cell line N_{eff} of radiation resistance $D_{0,eff}$ can describe the dose response relation rather well, but not the cell survival (cf. Fig. 4). For that, both the resistant and sensitive compartments are needed. Interestingly, the tumor control at its steepest region goes from almost zero to unity over a dose range of $eD_{0,eff}$ or about $2.7D_{0,eff}$. In reality, it does not reach unity until very high doses, since there is always a finite probability that a single tumor clonogen may have been missed.

Therapy optimization

Once a library of dose–response relations for tumors and normal tissues is available, it is possible to use these parameters for a more accurate biological optimization of the treatment plan for a given patient. For example, such a treatment plan developed for a prostate patient using intensity-modulated radiation therapy (IMRT) is shown in Fig. 10. In this case, optimization was performed in a way that the probability to cure the patient without inducing

Fig. 10 Dose distribution after biologically optimized dose delivery where both the angle of incidence and the intensity modulation of each beam was optimized. With IMRT, it is seen that at the same time as the prostate gets a high and sufficiently uniform dose, both the rectum and bladder are well protected by the intensity-modulated dose delivery in all planes through the tumor, and the complication-free cure is more than doubled compared to a conformal treatment with uniform beams. The optimal shift in the angle of incidence for the uniformly distributed beams are indicated, in this case resulting in a 3% increase in complication-free cure relative to uniformly distributed beams



severe normal tissue damage (P_+) was maximized based on an assumed correlation between tumor and normal tissue response:

$$P_+ = P_B - P_I, \quad (26)$$

where P_I is the probability for Injury, and P_B is the probability for Beneficial treatment sometimes called NTCP (Normal Tissue Complication Probability) or TCP (Tumor Control Probability), respectively (Källman et al. 1992; Brahme 1999). If P_I and P_B were truly independent processes, P_+ would instead be given by $P_+ = P_B(1 - P_I)$. However, this is generally not the case, since both get simultaneously a high dose and the genetic makeup of the tumor is very similar to that of the normal tissues, even if a hand full of genes are mutated in the tumor (Hanahan and Weinberg 2000; Ågren et al. 1990; Ågren Cronqvist et al. 1995; Brahme 2000). Interestingly, angle-of-incidence optimization was used in Fig. 10 resulting in a higher complication-free cure compared to that obtained if fixed standard angles were used. It is evident that rectum and bladder are well saved in this plan by biologically optimized IMRT, while at the same time the large prostate gets a sufficiently high and sufficiently uniform dose.

Actually, an even more refined optimization procedure is available nowadays which is called the P_{++} optimization strategy. This procedure starts with a regular P_+ optimization that defines the optimal \hat{P}_+ as in Fig. 10. Then a second optimization process is started where the injury to normal tissues is minimized under the constraint that P_+ is not significantly reduced from its peak value \hat{P}_+ (Fig. 11). This process allows the probability of injury to be reduced by about 3%, while the fraction of patients with

complication-free cure is reduced by much less than a percent ($\approx 0.3\%$). This result can be achieved since the P_+ curve shows a rather shallow maximum and, thus, a small dose reduction will reduce the probability for injury, P_I , significantly without reducing P_+ much.

A further improvement has recently been achieved by PET-CT imaging of the patient's individual tumor burden (Brahme 2003a, b). This approach is called BIOART for "Biologically Optimized 3-Dimensional in-vivo Predictive Assay based Radiation Therapy" and quantifies the tumor response based on PET-CT imaging during the first week of therapy. By this approach, P_B can be determined from the patient's individual response whereas P_I is taken from historical data. This obviously improves the accuracy of the treatment optimization significantly, since the major uncertainty is due to the large variability in tumor responsiveness between different patients, whereas their normal tissue responses generally varies less.

Conclusions

As discussed earlier, the actual radiation response of a tumor and surrounding normal tissues is a rather complex function of sub-cellular mechanisms and of tissue organization. An accurate description of these responses is essential to be able to perform an accurate treatment optimization. Obviously, in more complex situations, for example if a lung tumor is located close to the heart, the organ responses may interact. This may further complicate the situation, since the resultant lung damage will reduce the blood flow to the heart, which in turn may pump less

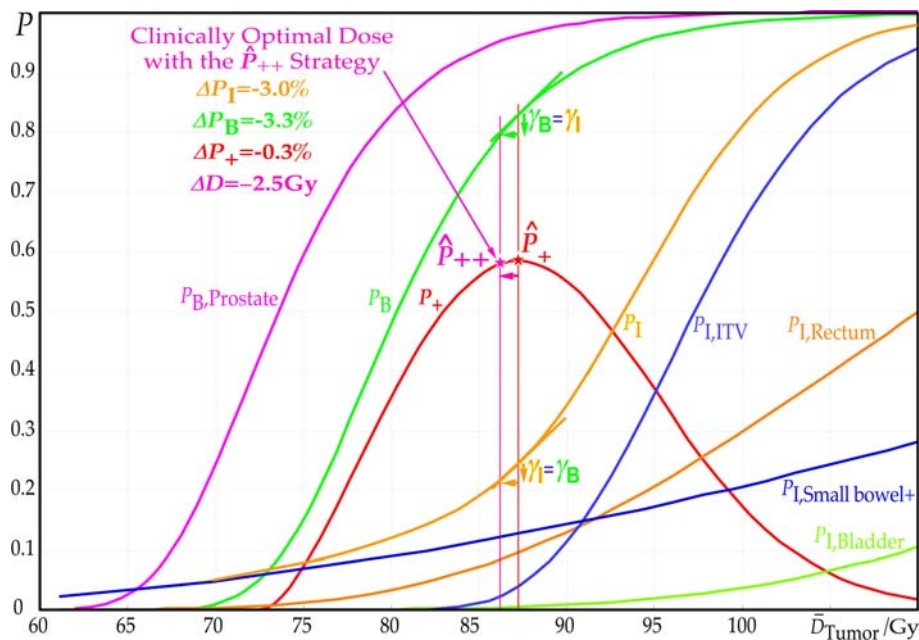


Fig. 11 The P_{++} optimization strategy applied on the prostate case in Fig. 10 allows biological optimization of the complication-free cure followed by a constrained normal tissue damage minimization. This reduces the risk for injury substantially (3%) without losing much of the complication-free cure (0.3%), due to the shallow peak of the bell-shaped P_+ curve. It therefore results in a quasi-simultaneous P_{benefit} and P_+ maximization and a constrained P_{injury} minimization. It

blood to the lung, due to its own damage and since it is receiving less oxygen from the lung. Thus, a rather complex interaction of radiation responses may occur. However, such complex interactions are not so common and a good treatment optimization can be achieved particularly by the BIOART approach. The optimal dose distribution obtained will then be close to the ideal one, although the exact absolute dose level may not be known exactly. However, this is a minor problem since the precise dose level should be selected in close collaboration with the responsible clinician. By the BIOART approach, considerable improvements in complication-free cure is therefore expected. It is remarkable that the team at the Memorial Sloan Kettering Cancer Center has been able to increase the 5-year biochemical relapse-free control of advanced prostate cancer (PSA > 20) from 21% by conformal therapy to 47% by physically optimized IMRT, at the same time as the complications were reduced from 17 to 4% (Zelefsky et al. 2006). Even more should be in reach by a more strict biological optimization. The corresponding figure for carbon ion therapy at the National Institute for Radiological Sciences in Japan is for example 89% (Ishikawa et al. 2006), indicating the considerable improvements in treatment outcome in reach with the light ions. The improvement in this case was largely due to a hypoxic or otherwise radiation-resistant tumor which can be

may thus be more clinically advantageous to lower the dose from that at the P_+ peak to the P_{++} position, in order to avoid the increased risk for severe damage at the 2.5 Gy higher dose level at the peak. γ_B and γ_I are the normalized dose–response gradients of the benefit and injury curves. P_{ITV} is the probability of injury in the internal target volume (target plus set-up margin)

effectively cured by the high-LET Bragg peaks without getting normal tissue damage since the low-LET plateau region has both a low RBE and a low dose. With IMRT and light ions, we thus have new very effective tools to cure most of our advanced tumors preferably using biologically optimized treatment planning based on the presently described procedures.

References

- Adamus-Górka M, Mavroidis P, Brahme A, Lind BK (2008) The dose-response relation for rat spinal cord paralysis analyzed in terms of the effective size of the functional subunit. *Phys Med Biol* 53:6533–6547
- Amundson SA, Bittner M, Fornace Jr AJ (2003) Functional genomics as a window on radiation stress signaling. *Oncogene* 22:5828–5833
- Brahme A (1999) Optimized radiation therapy based on radiobiological objectives. *Sem Oncol* 9:35–47
- Brahme A (2000) Development of radiation therapy optimization. *Acta Oncol* 39:579–595
- Brahme A (2003a) Biologically optimized 3-dimensional in vivo predictive assay based radiation therapy using positron emission tomography-computerized tomography imaging. *Acta Oncol* 42:123–136
- Brahme A (2003b) Fractionation & biologically optimized imrt using in vivo predictive assay based radiation therapy (bioart). *Acta Oncol* 42:123–136

- Brahme A (2004) Recent advances in light ion radiation therapy. *Int J Rad Onc Biol Phys* 58:603–616
- Brahme A, Rydberg B, Blomquist P (1997) Dual spatially correlated nucleosomal double strand breaks in cell inactivation. In: *Microdosimetry: an interdisciplinary approach*. The Royal Society of Chemistry, Philadelphia, pp 125–128
- Curtis SB (1986) Lethal and potential lethal lesions induced by irradiation: a unified repair model. *Radiat Res* 106:252–270
- Fei P, El-Deiry W (2003) P53 and radiation response. *Oncogene* 22:5774–5783
- Guerrero M, Allen Li X (2004) Extending the linear-quadratic model for large fraction doses pertinent to stereotactic radiotherapy. *Phys Med Biol* 49:4825–4835
- Hanahan D, Weinberg R (2000) The hallmarks of cancer. *Cell* 100:57–70
- Hirokawa N, Takemura R (2005) Molecular motors and mechanisms of directional transport in neurons. *Nature Rev* 6:201–214
- Hoeijmakers JHJ (2001) Genome maintenance mechanisms for preventing cancer. *Nature* 411:366–374
- Huang L, Snyder AR, Morgan WF (2003) Radiation-induced genomic instability and its implications for radiation carcinogenesis. *Oncogene* 22:5848–5854
- Ishikawa H, Tsuji H, Kamada T, Yanagi T, Mizoe J, Kanai T, Morita S, Wakatsuki M, Shimazaki J, Tsujii H (2006) Carbon ion radiation therapy for prostate cancer: results of a prospective phase ii study. *Radiother Oncol* 81:57–64
- Kappos W, Pohlit W (1972) A cybernetic model for radiation reactions in living cells. *Int J Radiat Biol* 22:51–65
- Källman P, Ågren AK, Brahme A (1992) Tumour and normal tissue responses to fractionated non-uniform dose delivery. *Int J Radiat Biol* 62:249–262
- Lind BK, Brahme A (2007) The radiation response of heterogeneous tumors. *Phys Med* 23:91–99
- Lind BK, Persson LM, Edgren MR, Hedlöf I, Brahme A (2003) Repairable conditionally repairable damage model based on dual poisson processes. *Radiat Res* 160:366–375
- Lindborg L, Brahme A (1990) Influence of microdosimetric quantities on observed dose-response relationships in radiation therapy. *Radiat Res* 124:S23–S28
- Marples B, Wouters BG, Collis SJ, Chalmers AJ, C JM (2004) Low-dose hyper-radiosensitivity: a consequence of ineffective cell cycle arrest of radiation-damaged g2-phases cells. *Radiat Res* 161:247–255
- Michalik V, Frankenberg D (1994) Simple and complex double-strand breaks induced by electrons. *Adv Space Res* 14:235–248
- Nakamura Y (2004) Isolation of p53-target genes and their functional analysis. *Cancer Sci* 95:7–11
- Park C, Papiem L, Zhang S, Story M, Timmerman R (2008) Computation of cell survival in heavy ion beams for therapy. *Int J Rad Onc Biol Phys* 70:847–852
- Scholz M, Kellerer A, Kraft-Weyrater W, Kraft G (1997) Computation of cell survival in heavy ion beams for therapy. *Radiat Environ Biophys* 36:59–66
- Svensson H, Ringborg U, Näslund I, Brahme A (2004) Development of light ion therapy at the karolinska hospital and institute. *Radiother Oncol* 74:206–210
- Tachibana A (2004) Genetic and physiological regulation of non-homologous end-joining in mammalian cells. *Adv Biophys* 38:21–44
- Takakura K, Takahashi M, Aoki M, Furusawa Y (2004) Mechanism of apoptosis induction in cultured cells irradiated with high let heavy-ion radiation. In: *Yearly Report by NIRS* pp 107–108 NIRS, Tokyo
- Tilikidis A, Brahme A (1994) Microdosimetric description of beam quality and biological effectiveness in radiation therapy. *Acta Oncol* 33:457–469
- Tobias CA (1985) The repair-misrepair model in radiobiology. *Radiat Res* 104:77–95
- Ward JF (1984) The complexity of DNA damage: relevance to biological consequences. *Int J Radiat Biol* 66:427–432
- Wouters BG, Brown JM (1997) Cells at intermediate oxygen levels can be more important than the “hypoxic fraction” in determining tumor response to fractionated radiotherapy. *Radiat Res* 147:541–550
- Xu B, Kim ST, Lim DS, Kastan MB (2002) Two molecularly distinct g2/m checkpoints are induced by ionizing irradiation. *Mol and Cell Biol* 22:247–255
- Zelefsky M, Chan H, Hunt M, Yamada Y, Shippy AHA (2006) Long-term outcome of high dose intensity modulated radiation therapy for patients with clinically localized prostate. *cancer J Urol* 176:1415–1419
- Ågren AK, Brahme A, Thureson I (1990) Optimization of uncomplicated control for head and neck tumors. *Int J Rad Onc Biol Phys* 19:1077–1085
- Ågren Cronqvist AK, Källman P, Turesson I, Brahme A (1995) Volume and heterogeneity dependence of the dose-response relationship for head and neck tumours. *Acta Oncol* 34:851–860